Journal of Energy Chemistry 57 (2021) 206–211

Contents lists available at ScienceDirect

Journal of Energy Chemistry

journal homepage: www.elsevier.com/locate/jechem

http://www.journals.elsevier.com/journal-of-energy-chemistry/

Immobilizing polysulfide jointly via chemical absorbing and physical blocking in polytungstates-embedded carbon nanofibers

Yanmei Nie [a], Lei Tan [a,c], Guangchao Li [a], Sanghao Li [a], Jun Yan [a,b,*], Jiexi Wang [a,c,*]

[a] College of Chemistry and Chemical Engineering & School of Metallurgy and Environment, Central South University, Changsha 410083, Hunan, China
[b] Hunan Provincial Key Laboratory of Chemical Power Sources, Central South University, Changsha 410083, Hunan, China
[c] Engineering Research Center of the Ministry of Education for Advanced Battery Materials, Central South University, Changsha 410083, Hunan, China

ARTICLE INFO

Article history:
Received 30 June 2020
Revised 17 August 2020
Accepted 18 August 2020
Available online 28 August 2020

Keywords:
Lithium-sulfur batteries
Polysulfides
Polyoxometalates
Carbon nanofibers

ABSTRACT

Lithium-sulfur (Li-S) battery is regarded as one of the most fascinating candidates for energy storage due to its dominant advantage of high energy density. However, the shuttling effect of soluble polysulfides and low electrical conductivity of sulfur and Li_2S still hinder its commercialization. In this work, high electrical-conductive carbon nanofibers (CNFs) with uniformly embedded polytungstates (HPW@CNFs) are proposed for advanced Li-S batteries. $H_3PW_{12}O_{40}$ (HPW) is a kind of molecular nano-sized metal cluster which contains rich Lewis acid/base sites that can stabilize polysulfide effectively through chemical bonding, while CNFs play the role of physical barriers for polysulfides and transmission channel for electrons. The HPW@CNFs/S cathode shows an ultra-stable cycling performance with extremely small decay rate of 0.015% per cycle over 400 cycles at 0.5 C.

1. Introduction

Lithium ion batteries (LIBs), a typical commercialized energy system that has revolutionized portable electronic devices since 1991, could not quite satisfy the steadily increasing energy consumption due to the development of industrialization and economy [1,2]. The exploration of advanced energy storage systems with higher energy densities is overwhelming among researchers [3]. Lithium-sulfur (Li-S) battery is a new class of rechargeable batteries whose theoretical specific capacity and energy density are as high as 1675 mAh g^{-1} and 2600 Wh kg^{-1}, respectively [4–6]. In addition, sulfur is abundant in nature, cheap, non-toxic and environmentally friendly [7]. All the above endowed advantages make Li-S battery a hotspot for the next-generation of energy storage systems [8,9]. However, Li-S batteries are still not primed for commercialization due to several inherent challenges, like poor electrical conductivity of sulfur and its discharge products (Li_2S_2/Li_2S), big volumetric expansion high up to 79% from sulfur (2.07 g cm^{-3}) to Li_2S (1.66 g cm^{-3}), as well as severe side reactions between mobile soluble polysulfides [Li_2S_x (x = 4–8)] and lithium anode which produce insoluble Li_2S and Li_2S_2 on metallic lithium surface [10]. These problems trigger poor rate performance, fast capacity attenuation and low coulombic efficiency. To handle these issues, great efforts have been made, especially preventing polysulfide from shuttling [11]. Various materials ranging from polymeric (polypropylene, polyaniline), inorganic (metal oxide, metal sulfide, metal cluster) and carbonaceous hosts have been explored to confine polysulfide [12–16]. Compared with normal porous carbon encapsulating sulfur through physical adsorption to limit part of polysulfide from shuttling, surface functionalized carbonaceous material and inorganic compounds prohibiting polysulfide from shuttling through chemical adsorption or chemical bonding are prevailing among researchers [17–20]. When compared with conventional hosts, polar hosts like metal oxides or polyoxoanions which can provide abundant Lewis acid-base sites have been proved to have stronger adsorption, better electric contact and faster conversion ability among polysulfides [21].

Polyoxometalates (POMs), a class of metal–oxygen clusters based on early transition metals (Mo, W, V, Nb, Ta), have attracted increasing attention as inorganic hosts for Li-S batteries due to their unparalleled properties originated from controllable size and diversified structure [22–24]. POMs with abundant surface oxygen atoms acting as Lewis base and metal atoms acting as Lewis acid, could effectively stabilize Li_2S_x (x = 4–8) moieties through chemical bonding [25]. However, the rational utilization of POMs remains plagued by instability and low conductivity

* Corresponding authors at: College of Chemistry and Chemical Engineering & School of Metallurgy and Environment, Central South University, Changsha 410083, Hunan, China.
E-mail addresses: yanjun@csu.edu.cn (J. Yan), wangjiexikeen@csu.edu.cn (J. Wang).

https://doi.org/10.1016/j.jechem.2020.08.032

[26,27]. $H_3PW_{12}O_{40}$ (HPW) is a classic keggin-type POMs which not only is capable of transferring multielectron reversibly but also maintains structural stability in wide range of soluble solvents [28,29]. Although research about polyoxometalates for Li-S battery is scanty, there are still several types of stable polyoxometalates that have been proved to be good hosts for sulfur or even as separator coating layers for Li-S battery according to previous studies [30,31]. HPW is selected as inorganic hosts for sulfur due to their advantages of unique nano-sized, easily accessible and chemical stable. However, the low conductivity of both sulfur and HPW is still intractable. Moreover, HPW separated out from solution often aggregates to bulk sub-micron grade powders which can impede the inherent advantages of nanostructure. Hybrid polyanions with carbonaceous substrate material is common for the enhancement of uniform distribution and conductivity [32,33]. Carbon nanofibers (CNFs), excellent conductive additives with large surface areas and structural stability, have been widely used in electrochemical energy storage devices [34,35].

As a versatile and viable technique for generating ultrathin carbon fibers, here electrospinning is employed for generating HPW uniformly embedded CNFs (HPW@CNFs) [36]. Further, HPW@CNFs was loaded with sulfur (HPW@CNFs/S) as cathode for Li-S battery. In this composite, HPW are homogenously dispersed in the CNFs, so that the electronic conductivity is much enhanced and the aggregation of HPW is well suppressed. As a result, rich chemical bonding of HPW with sulfur is expected. Besides, CNFs is also a good matrix for physical absorption of sulfur due to their abundant porous structure [37]. With jointly contribution of chemical absorbing and physical blocking, the shuttling of polysulfide could be well prohibited.

2. Experimental

2.1. Materials

All the reagents used were associated to analytical grade without any further purification and provided by the commercial suppliers.

2.2. Synthesis of HPW

HPW was synthesized according to a previous study [38]. Briefly, 100 g $Na_2WO_4{\cdot}2H_2O$ was dissolved in 100 mL distilled boiling water to form a clear solution under vigorous stirring, then 10 mL of 85% H_3PO_4 was added. After that, 80 mL concentrated hydrochloric acid (12 mol L^{-1}) was added drop wise. Four hours later, coarse product was collected by filtration and re-dissolved in deionized water. Excess diethyl ether and concentrated hydrochloric acid were added till the solution was divided into three layers. Finally, transparent crystal of HPW was collected through slow evaporation from the bottom layer and dried at room temperature.

2.3. Synthesis of HPW@CNFs and CNFs

Polyacrylonitrile (PAN) based nanofibers were prepared by coaxial electrospinning technique. Firstly, PAN (M_w = 1.3 × 10^6 g mol^{-1}) powder was added into 10 mL *N,N*-dimethyformamide (DMF) and stirred at 80 °C for 2 h to obtain a homogeneous solution. Then, 0.576 g of HPW was added. After vigorous stirring overnight, homogeneous solution of HPW-PAN/DMF was obtained. Freshly prepared precursor solution was transferred into a 10 mL plastic syringe and injected with a feeding rate of 6 μL min^{-1}. A voltage of 12 kV (high voltage: 10 kV; low voltage −2 kV) was supplied between the collector and the metal nozzle. A rotating aluminum drum was grounded and set as the collector with a distance of 10 cm to the needle tip to obtain HPW embedded nanofibers. After that, the prepared sample was peeled off from Al foil and dried in vacuum at 80 °C overnight. Then the nanofibers were stabilized at 280 °C (Air atmosphere) for 2 h with a heating rate of 5 °C min^{-1}. Finally, the stabilized nanofibers were carbonized at 600 °C under Ar atmosphere to obtain the composite (HPW@CNFs). CNFs were synthesized similar to HPW@CNFs without adding HPW.

2.4. Synthesis of Li_2S_6

Brownish-red Li_2S_6 solution was prepared by reacting sublimed sulfur with appropriate amount of Li_2S (S:Li_2S = 5:1 in mole) in DOL/DME solution (1:1 in volume) in glove box (O_2 < 0.1 ppm, H_2O < 0.1 ppm).

2.5. Synthesis of HPW@CNFs/S and CNFs/S cathodes

HPW@CNFs/S composite was obtained by mixing sulfur and HPW@CNFs with a weight ratio of 3:1. Then the mixture was transferred into the reaction kettle and heated at 155 °C for 12 h. The HPW@CNFs/S cathode was fabricated by pasting the sulfur slurry (mass ratio: 75% HPW@CNFs/S, 15% ketjen black, and 10% LA132) onto Al foil and dried at 60 °C overnight in a vacuum oven. Synthesis of CNFs/S cathode was similar to HPW@CNFs/S cathode except sulfur was mixed with pure CNFs.

2.6. Materials characterization

X-ray diffraction (XRD), TTRIII X-ray diffractometer with Cu-K_α radiation, was employed to character the structure of samples. The detailed structural information of CNFs and HPW@CNFs was revealed by X-ray photoelectron spectroscopy (XPS, Perkin-Elmer, PHI 5600). The micro-morphologies of materials were detected by scanning electron microscope (SEM, JEOL, JSM-5612LV) and field emission transmission electron microscope (FE-TEM, Titan, G2 60-300). Especially, the element distribution in the substrate was collected by the energy dispersive X-ray spectroscopy (EDS). UV/Vis absorption spectra were measured with a SHIMADZU UV2600 UV/Vis spectrophotometer. Thermogravimetric analyses were performed with a NETZSCH STA 449C TGA instrument, inflowing Ar with a heating rate of 10 °C min^{-1}.

2.7. Electrochemical tests

The sulfur electrodes were punched into a 12 mm disks in diameter, in which the loading mass was controlled around 1.0–1.2 mg cm^{-2} and 2.3–2.5 mg cm^{-2}, respectively. Coin-type cells were assembled in the glove box filled with Ar atmosphere (O_2 < 0.1 ppm, H_2O < 0.1 ppm). The electrolyte was composed of 1 M lithium bis(trifluoromethanesulfonyl) imide (LiTFSI) in a solvent of 1,3-dioxolane (DOL) and dimethoxymethane (DME) (1:1 in volume) with 2% $LiNO_3$. The cyclic voltammetry (CV) plots and electrochemical impendence spectroscopy (EIS) tests were investigated by CHI660d electrochemical working station. A Land battery test system was used to perform charge/discharge measurements in the voltage window of 1.7–2.8 V at various current rates (1C is equivalent to 1675 mA g^{-1}).

3. Results and discussion

HPW@CNFs/S cathode was prepared through electrostatic spinning employing polyacrylonitrile (PAN) and HPW as precursors with further annealing and melt-fusing process. As schematically

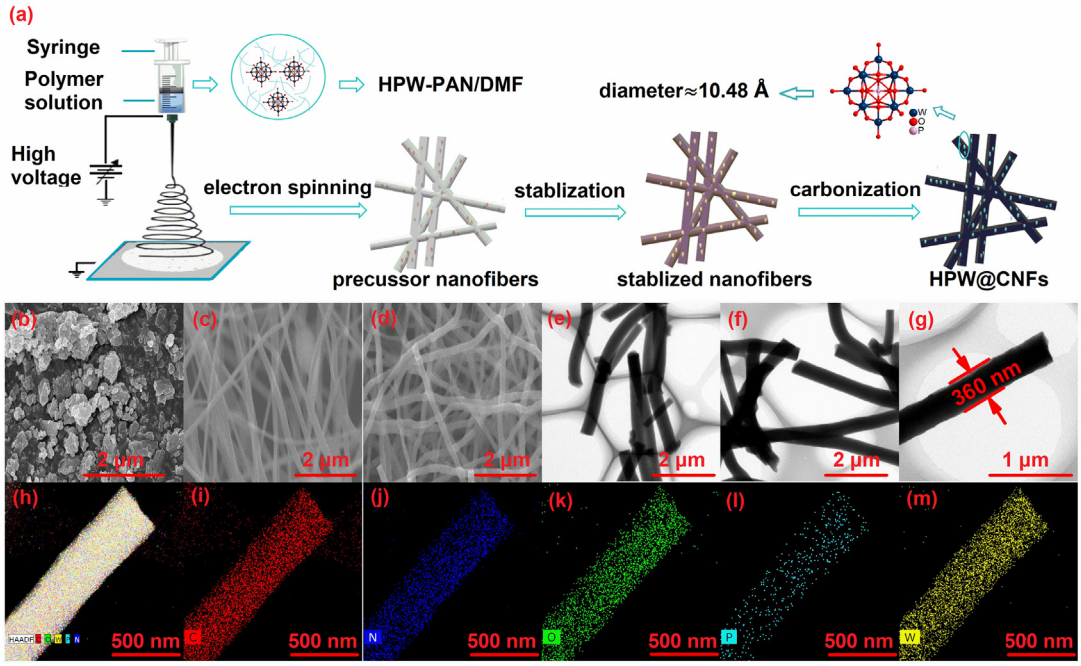

Fig. 1. (a) Schematic illustration of the synthetic process of HPW@CNFs, SEM images of (b) HPW, (c) CNFs, (d) HPW@CNFs, (e) TEM image of CNFs, (f, g) TEM micrographs of HPW@CNFs, (h-m) HADDF and EDS mapping of HPW@CNFs.

illustrated in Fig. 1(a), coaxial electrospinning was applied to synthesize HPW@PAN nanofibers. Then the precursor (electrospun nanofibers) was stabilized in air and carbonized under Ar. Electrostatic spinning not only solves the problem of low conductivity but also disperses HPW particles into CNFs evenly. CNFs without the addition of HPW were synthesized similarly for comparison. SEM image reveals that the solid form of HPW separate out as submicron or even micron grade block crystal (Fig. 1b). SEM (Fig. 1c and d) and TEM (Fig. 1e and f) images display a similar morphology of CNFs and HPW@CNFs. Fig. 1(g) shows that the diameter of HPW@CNFs is about 360 nm. It is obvious that HPW (molecular diameter ≈1 nm) has been embedded into CNFs evenly through electrospinning and has no distinct effect on the fiber-like shape [39,40]. HADDF image together with elemental mappings (Fig. 1h–m) demonstrates that phosphorus (P), tungsten (W), oxygen (O), carbon (C) and nitrogen (N) atoms are uniformly distributed, indicating good dispersion of HPW in CNFs as well. Benefiting from this, the as-prepared HPW@CNFs has excellent electronic conductivity and increased polysulfides adsorption sites, which is conducive to promoting the electrochemical performance of Li-S battery.

As shown in the XRD patterns (Fig. 2), after stabilized at 280 °C for 2 h, the characteristic peaks of hydrated HPW maintain. After dehydrating under Ar atmosphere at 600 °C for 2 h, dehydrated HPW is obtained. Though covered up by two broad peaks around 25° and 44° which are separately assigned to (002) and (100) diffraction of carbon material, the weak characteristic peaks of HPW retain in the XRD pattern of HPW@CNFs.

X-ray photoelectron spectroscopy (XPS) was carried out to obtain the element composition and valence state of HPW@CNFs. The XPS survey spectrum of HPW@CNFs displays the presence of a set of peaks corresponding to C 1s, N 1s, O 1s, P 2p, W 4p, W 4d and W 4f (Fig. 3a). As for the high-resolution C 1s spectrum (Fig. 3b), peaks center at 284.8, 286.6, 288.9 and 290.9 eV are attributed to C—C bond, C—O bond, O=C—N bond and O=C—O bond, separately. As for the high resolution of N 1 s peaks (Fig. 3c), four peaks center at 398.5, 400.1, 401.5 and 405.3 eV are correspondingly assigned to pyridinic-N, pyrrolic-N, graphitic-N and oxidized-N [41,42], and the percentage is 58.1%, 32.0%, 2.1% and 7.8%, accordingly. The high percentage (up to 90%) of pyridinic-N and pyrrolic-N is favorable for bettering cycling performance, because they are the most stable configurations for adsorbing polysulfides among all the nitrogen containing functional groups [43,44]. W 4f spectrum (Fig. 3d) is segmented into two peaks center at 36.4 (W 4f 7/2) and 38.4 eV (4f 5/2). High resolution of C 1s and N 1s peaks of CNFs are displayed in Fig. 3(e and f), respectively. After adsorbing Li_2S_6, the intensity of the former peaks recedes and two additional peaks at 37.4 and 34.9 eV belonging to W 4f 5/2 and W 4f 7/2 are discovered (Fig. 3g), the decreased binding energies of W 4f core levels is attributed to S- rather than O-bonding [28,45,46]. This suggests that W has a strong chemical affinity for sulfur in the polysulfides. It also verifies the chemical adsorption capability of HPW@CNFs for polysulfides from another side. UV–Vis spectra of Li_2S_6 solution before and after absorbed by the samples is shown in Fig. 3(h). When compared with the decline of the adsorption intensity in CNFs/Li_2S_6 solution, the adsorption intensity of S_6^{2-} species at 250 and 300 nm decreases more evidently in HPW@CNFs/Li_2S_6 solution [47,48], which proves the strong interaction between HPW@CNFs and polysulfides. Likewise, the color variation from bright yellow to nearly colorless of Li_2S_6 solution demonstrated in the inserted digital graph proves obvious adsorption ability of HPW@CNFs for polysulfides. According to the calculation of weight loss from 160 to 300 °C in the TGA curves, the active sulfur contents are approximately 74.9% for HPW@CNFs/S and 71.4% for CNFs/S (Fig. 3i).

Fig. 4(a and b) show the cycle performance of Li-S cells at 0.2 C and 0.5 C (1 C = 1675 mA g^{-1}) using HPW@CNFs/S and CNFs/S cathode. Li-S cell assembled with HPW@CNFs/S cathode manifests larger specific capacity and higher capacity retention than CNFs/S. The initial discharge capacity at 0.2 C for HPW@CNFs/S is 974 mAh g^{-1} and remains 909 mAh g^{-1} after cycling for 100 cycles, with an average capacity decay rate about 0.067% per cycle and 93.20% capacity retention. In comparison, the specific capacity of CNFs/S cathode at 0.2 C for the 1st and 100th cycle is 663 and

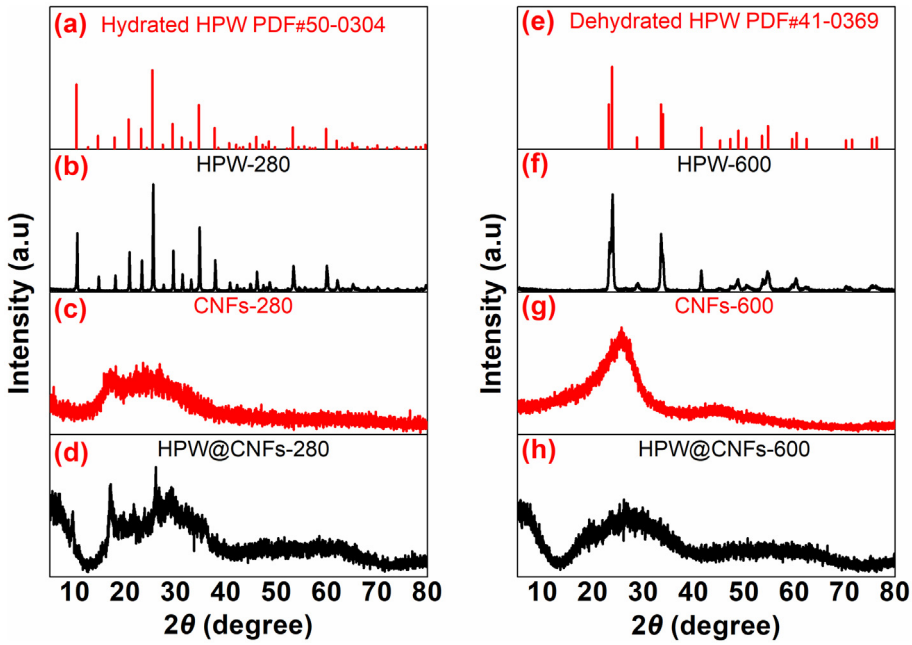

Fig. 2. XRD patterns. (a) Standard PDF of hydrated HPW; (b) HPW stabilized at 280 °C for 2 h; (c) CNFs stabilized at 280 °C for 2 h; (d) HPW@CNFs stabilized at 280 °C for 2 h; (e) Standard PDF of dehydrated HPW; (f) HPW annealed at 600 °C for 2 h; (g) CNFs annealed at 600 °C for 2 h; (h) HPW@CNFs annealed at 600 °C for 2 h.

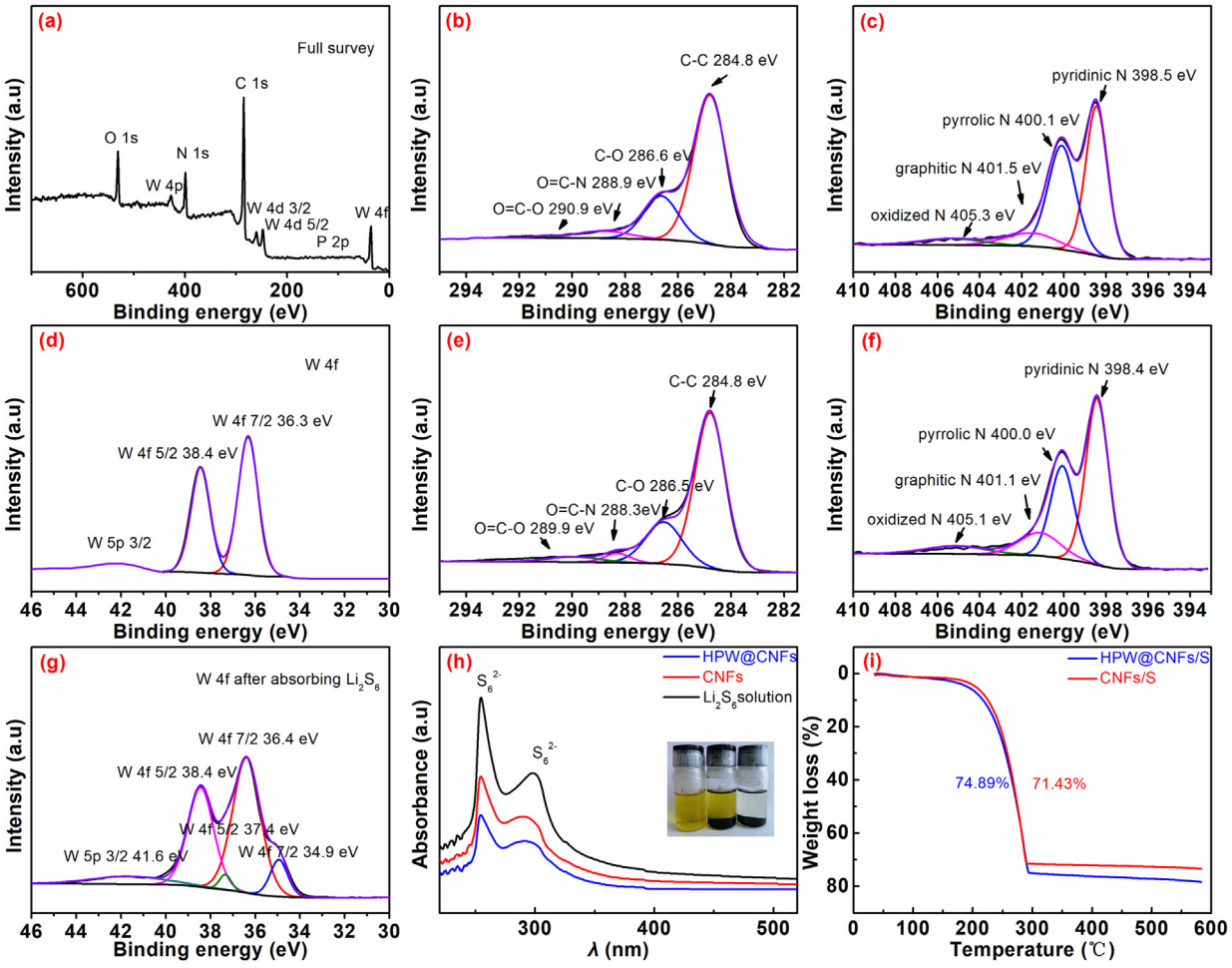

Fig. 3. (a–g) XPS spectra: (a) Full survey of HPW@CNFs, (b) C 1 s of HPW@CNFs, (c) N 1s of HPW@CNFs, (d) W 4f of HPW@CNFs, (e) C 1s of CNFs, (f) N 1s of CNFs, (g) W 4f of HPW@CNFs after absorbing Li_2S_6; (h) UV-Vis spectra of Li_2S_6 solution, Li_2S_6 + CNFs and Li_2S_6 + HPW@CNFs; inset: Digital photos demonstrating color of Li_2S_6 solution (left: without absorbent; middle: absorbed by CNFs; right: absorbed by HPW@CNFs); (i) TGA curves of HPW@CNFs/S and CNFs/S.

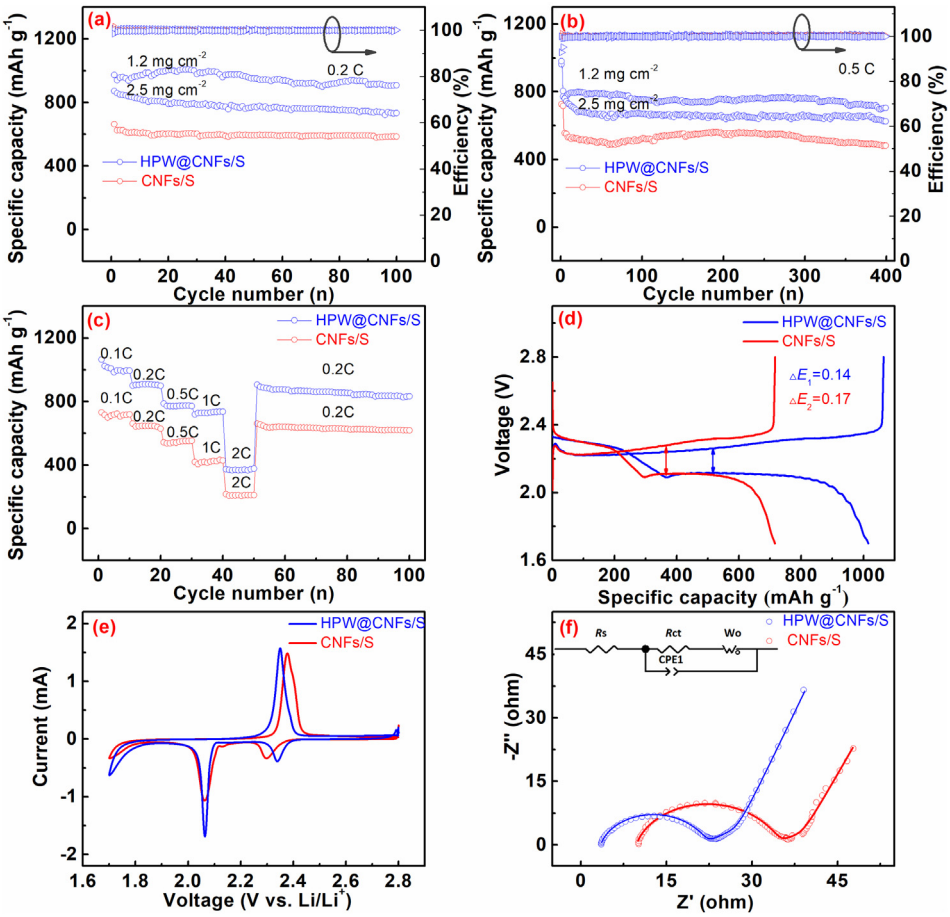

Fig. 4. Electrochemical performance of HPW@CNFs/S and CNFs/S in Li-S batteries. (a) Cycling performance at 0.2 C; (b) cycling performance at 0.5 C, (c) rate performance; (d) typical galvanostatic charge–discharge voltage profiles at 0.2 C; (e) CV curves; (f) Nyquist plots.

587 mAh g^{-1}, respectively, accompanied by an average capacity decay rate of 0.12% per cycle and capacity retention of 88.40%. Moreover, the HPW@CNFs/S cathode also shows ultra-stable cycle performance at high-rate, delivering a specific capacity of 751 mAh g^{-1} at 0.5 C and maintaining 706 mAh g^{-1} after 400 cycles along with the average decay rate of 0.015% per cycle. While the CNFs/S cathode starts at 565 mAh g^{-1} and ends up in 479 mAh g^{-1} after 400 cycling together with the average decay rate of 0.038% per cycle. When the average sulfur loading is increased to 2.5 mg cm^{-2}, the initial discharge capacity of HPW@CNFs/S cathode cycling at 0.2C and 0.5C with is 872 mAh g^{-1} and 776 mAh g^{-1}. After cycling for 100 cycles and 400 cycles, the specific capacity remains 734 mAh g^{-1} and 625 mAh g^{-1}, respectively. Furthermore, HPW@CNFs/S cathode shows excellent rate capability (Fig. 4c). Stable specific capacities of 1020, 910, 780, 730 and 380 mAh g^{-1} are delivered when tested at 0.1, 0.2, 0.5, 1, and 2 C respectively. The discharge capacity decreases gradually with the increasing of the current density. After several cycles, the specific capacity of 0.2C goes back to the same level nearly without fading. In contrast, CNFs/S cathode exhibits 710, 650, 540, 420, 210 mAh g^{-1} at identical testing conditions. Typical charge–discharge profiles of Li-S cells are presented in Fig. 4(d). For the discharging process, the high voltage plateaus around 2.4 V and comparatively low voltage plateaus at 2.1 V are attributed to the reduction peaks of elemental sulfur (S_8) to a number of higher ordered polysulfides (Li_2S_x, x = 4–8) species and the conversion of high ordered Li_2S_x (x = 4–8) to accordingly short chain Li_2S_2 or Li_2S. For the subsequent charging process, a long plateau corresponding to the oxidation of short chain Li_2S_2/Li_2S is observed [5,8]. It also can be seen from Fig. 4(d) that HPW@CNFs/S manifests smaller polarization when compared with CNFs/S. For HPW@CNFs/S, the half-capacity voltage difference ($\triangle E_1$) is 0.14 V while that of CNFs/S ($\triangle E_2$) is 0.17 V. This reveals that HPW-embedded CNFs helps to enhance the sluggish redox reaction kinetics and suppress polarization. It has been proved by XPS result and UV spectra that inorganic HPW successfully confined the shuttling effect of LiPS and accelerated the conversion process of LiPS to sulfur. As a result, the sluggish electrochemical reaction kinetics was improved and polarization was suppressed [49]. Fig. 4(e) shows the CV profiles of HPW@CNFs/S and CNFs/S at a scan rate of 0.2 mV s^{-1}. The high voltage cathodic peaks of HPW@CNFs/S and CNFs/S locate at 2.33 and 2.29 V, and the low-voltage cathodic peaks center at 2.06 and 2.05 V, respectively. The anodic peaks of HPW@CNFs/S and CNFs/S position at 2.35 and 2.38 V, separately. It can be concluded from CV profiles that higher cathodic peaks and lower anodic peak of HPW@CNFs further reflects a small polarization [48]. Nyquist plots of both samples before cycling are given in Fig. 4(f), in which the intercept on the real axis at high frequency is labelled as the interface resistance of electrolyte and electrode (R_s), and the diameter of semicircle refers to the charge transfer resistance (R_{ct}). Based on the fitting results, R_s of CNFs/S (10.1 Ω) is much higher than that of HPW@CNFs/S cathode (3.6 Ω), which may be contributed by the increased electrolyte viscosities resulted from dissolved polysulfides. R_{ct} of HPW@CNFs/S cathode (20.2 Ω) is less than that of CNFs/S cathode (25.1 Ω), which may be resulted from the electron-transferable HPW. All in all, lowered resistance,

suppressed polarization and stable cycling performance are achieved benefited from the excellent adsorption ability of HPW@CNFs to polysulfides.

4. Conclusions

In summary, HPW@CNFs/S cathode for Li-S battery has been successfully prepared through electrostatic spinning with further annealing and melt fusing process. The agglomeration of HPW was effectively suppressed and thus embedded into CNFs evenly. The prepared HPW@CNFs perfectly combined the advantages of high conductive carbonaceous materials and nano-sized POMs. Contributed by chemical absorbing and physical blocking originated from HPW and CNFs jointly, HPW@CNFs alleviated polysulfide diffusion and consequently improved specific capacity and enhanced the cycle stability of Li-S battery. An ultra-stable cycling performance with extremely small decay rate of 0.015% per cycle over 400 cycles at 0.5 C was achieved. The synthesis of HPW@CNFs provides an innovative approach and guidance for the development of POM-based materials for Li-S battery which are extremely important for the advancement of energy storage devices.

Declaration of Competing Interest

The authors declare that they have no known competing financial interests or personal relationships that could have appeared to influence the work reported in this paper.

Acknowledgments

This work was financially supported by the National Natural Science Foundation of China (Grant No. 51874360), the Program of Huxiang Young Talents (Grant No. 2019RS2002), the Innovation-Driven Project of Central South University (2020CX027) and the Recruitment Program of Global Youth Experts.

References

[1] B. Scrosati, J. Hassoun, Y.K. Sun, Energy Environ. Sci. 4 (2011) 3287–3295.
[2] J. Mei, T. Liao, L. Kou, Z. Sun, Adv. Mater. 29 (2017) 1700176.
[3] H.J. Peng, J.Q. Huang, Q. Zhang, Chem. Soc. Rev. 46 (2017) 5237–5288.
[4] S. Urbonaite, T. Poux, P. Novák, Adv. Energy Mater. 5 (2015) 1500118.
[5] M. Wild, L. O'Neill, T. Zhang, R. Purkayastha, G. Minton, M. Marinescu, G.J. Offer, Energy Environ. Sci. 8 (2015) 3477–3494.
[6] X. Chen, T. Hou, K.A. Persson, Q. Zhang, Mater. Today 22 (2019) 142–158.
[7] Z.W. Seh, Y. Sun, Q. Zhang, Y. Cui, Chem. Soc. Rev. 45 (2016) 5605–5634.
[8] S.H. Chung, A. Manthiram, Adv. Mater. 31 (2019) 1901125.
[9] A. Rosenman, E. Markevich, G. Salitra, D. Aurbach, A. Garsuch, F.F. Chesneau, Adv. Energy Mater. 5 (2015) 1500212.
[10] J. He, A. Manthiram, Energy Storage Mater. 20 (2019) 55–70.
[11] C. Deng, Z. Wang, S. Wang, J. Yu, J. Mater. Chem. A 7 (2019) 12381–12413.
[12] T.Z. Zhuang, J.Q. Huang, H.J. Peng, L.Y. He, X.B. Cheng, C.M. Chen, Q. Zhang, Small 12 (2016) 381–389.
[13] Y. Wei, Y. Yan, Y. Zou, M. Shi, Q. Deng, N. Zhao, J. Wang, C. You, R. Yang, Y. Xu, Electrochim. Acta 310 (2019) 45–57.
[14] K. Chen, Z. Sun, R. Fang, Y. Shi, H.M. Cheng, F. Li, Adv. Funct. Mater. 28 (2018) 1707592.
[15] W. Yang, W. Yang, A. Song, G. Sun, G. Shao, Nanoscale 10 (2018) 816–824.
[16] L. Tan, X. Li, Z. Wang, H. Guo, J. Wang, ACS Appl. Mater. Interfaces 10 (2018) 3707–3713.
[17] Y. Li, I.A. Murphy, Y. Chen, F. Lin, X. Wang, S. Wang, D. Hubble, S.H. Jang, K.T. Muller, C. Wang, A.K.Y. Jen, J. Yang, J. Mater. Chem. A 7 (2019) 13372–13381.
[18] J. Wu, Q. Ma, C. Lian, Y. Yuan, D. Long, Chem. Eng. J. 370 (2019) 556–564.
[19] J. Xu, W. Zhang, Y. Chen, H. Fan, D. Su, G. Wang, J. Mater. Chem. A 6 (2018) 2797–2807.
[20] V. Singh, A.K. Padhan, S.D. Adhikary, A. Tiwari, D. Mandal, T.C. Nagaiah, J. Mater. Chem. A 7 (2019) 3018–3023.
[21] P. Zeng, H. Yu, M. Chen, W. Xiao, Y. Li, H. Liu, J. Luo, J. Peng, D. Shao, Z. Zhou, Z. Luo, Y. Wang, B. Chang, X. Wang, J. Energy. Chem. 51 (2020) 21–29.
[22] N.I. Gumerova, A. Rompel, Nat. Rev. Chem. 2 (2018) 0112–0131.
[23] L. Chen, R. Luque, Y. Li, Chem. Soc. Rev. 46 (2017) 4614–4630.
[24] J. Friedl, M.V. Holland-Cunz, F. Cording, F.L. Pfanschilling, C. Wills, W. McFarlane, B. Schricker, R. Fleck, H. Wolfschmidt, U. Stimming, Energy Environ. Sci. 11 (2018) 3010–3018.
[25] J.C. Ye, J.J. Chen, R.M. Yuan, D.R. Deng, M.S. Zheng, L. Cronin, Q.F. Dong, J. Am. Chem. Soc. 140 (2018) 3134–3138.
[26] Z. Peng, Angew. Chem. Int. Ed. 43 (2004) 930–935.
[27] A. Proust, B. Matt, R. Villanneau, G. Guillemot, P. Gouzerh, G. Izzet, Chem. Soc. Rev. 41 (2012) 7605–7622.
[28] J. Meng, X. Wang, X. Yang, A. Hu, Y. Guo, Y. Yang, Appl. Catal. B 251 (2019) 168–180.
[29] W. Ma, Y. Xu, K. Ma, H. Zhang, Appl. Catal. A-Gen. 526 (2016) 147–154.
[30] N. Yan, W. Zhang, J. Shi, Y. Liu, H. Cui, Mater. Lett. 229 (2018) 198–201.
[31] W. Yao, L. Liu, X. Wu, C. Qin, H. Xie, Z. Su, ACS Appl. Mater. Interfaces 10 (2018) 35911–35918.
[32] M. Zhang, A.M. Zhang, X.X. Wang, Q. Huang, X. Zhu, X.L. Wang, L.Z. Dong, S.L. Li, Y.Q. Lan, J. Mater. Chem. A 6 (2018) 8735–8741.
[33] X. Lou, Q. Fu, J. Xu, X. Liu, C. Lin, J. Han, Y. Luo, Y. Chen, X. Fan, J. Li, ACS Appl. Nano Mater. 1 (2017) 183–190.
[34] M.A. Mazo, A. Tamayo, A.C. Caballero, J. Rubio, Carbon 138 (2018) 42–51.
[35] L. Zhen, Z. Jintao, L.X. Wen David, Angew. Chem. Int. Ed. 54 (2015) 12886.
[36] J. Xue, T. Wu, Y. Dai, Y. Xia, Chem. Rev. 119 (2019) 5298–5415.
[37] Y. Chen, X. Li, K.S. Park, J. Hong, J. Song, L. Zhou, Y.W. Mai, H. Huang, J.B. Goodenough, J. Mater. Chem. A 2 (2014) 10126–10130.
[38] H. Wu, J. Biol. Chem. 43 (1920) 188–220.
[39] J.F. Keggin, Nature 131 (1933) 908–909.
[40] A. Nisar, J. Zhuang, X. Wang, Adv. Mater. 23 (2011) 1130–1135.
[41] S. Akula, A.K. Sahu, ACS Appl. Mater. Interfaces 12 (2020) 11438–11449.
[42] Z. Pu, J. Zhao, I.S. Amiinu, W. Li, M. Wang, D. He, S. Mu, Energy Environ. Sci. 12 (2019) 952–957.
[43] J. Zhang, Y. Cai, Q. Zhong, D. Lai, J. Yao, Nanoscale 7 (2015) 17791–17797.
[44] J. Balach, H.K. Singh, S. Gomoll, T. Jaumann, M. Klose, S. Oswald, M. Richter, J. Eckert, L. Giebeler, ACS Appl. Mater. Interfaces 8 (2016) 14586–14595.
[45] K. Li, L. Yan, Z. Zeng, S. Luo, X. Luo, X. Liu, H. Guo, Y. Guo, Appl. Catal. B 156–157 (2014) 141–152.
[46] D. Wang, Q. Li, C. Han, Z. Xing, X. Yang, ACS Cent. Sci. 4 (2018) 112–119.
[47] C. Barchasz, F. Molton, C. Duboc, J.C. Lepretre, S. Patoux, F. Alloin, Anal. Chem. 84 (2012) 3973–3980.
[48] B. Cao, B. Li, Y. Hou, L. Mo, Y.C. Yin, ACS Appl. Mater. Interfaces 8 (2016) 27795–27802.
[49] B. Guan, Y. Zhang, L. Fan, X. Wu, M. Wang, Y. Qiu, N. Zhang, K. Sun, ACS Nano 13 (2019) 6742–6750.